A B-spline based and computationally performant projector for iterative reconstruction in tomography - Application to dynamic X-ray gated CT

Fabien Momey, Loïc Denis, Catherine Mennessier, Éric Thiébaut, Jean-Marie Becker, Laurent Desbat

A B-spline based and computationally performant projector for iterative reconstruction in tomography *Application to dynamic X-ray gated CT*

Fabien Momey, Loïc Denis, Catherine Mennessier, Éric Thiébaut, Jean-Marie Becker, Laurent Desbat

I. Introduction

ITERATIVE reconstruction methods for tomography have long proven their potential to enhance reconstruction quality, compared to the filtered backprojection (FBP) [2]. The drawback of iterative methods is their expensive computation time. However ongoing researches on algorithms and recent enhancements in computational power, call for a re-evaluation of the potential of iterative reconstruction in this domain.

Such methods require an accurate numerical modelization of the data acquisition process: the so-called *projector*. The representation of the object of interest (image) is the starting point of the projector. It is assimilated to a continuous function decomposed on a discrete basis of functions. The choice of this basis is essential for an accurate representation of the true function. Standard models such as *voxel driven* or *ray driven* [5] are based on raw samples, yielding modelization errors and artifacts on the reconstructed image. More advanced models, such as the recent *distance driven* [1] projector, define the function at any point considering staircase voxels, and thus make a better modelization. However such a basis of functions provides a coarse representation of the image because of its anisotropic behaviour, causing large modelization errors. Such issues can be dealt with the spherically symmetric volume elements, mostly known as blobs [7] [8] [9] [10] [11], but at the cost of increased complexity. Finally, for implementation purposes, the projection of the staircase voxel, in the *distance driven* model, is approximated, increasing its modelization errors.

We propose the use of B-splines as an alternative to both staircase voxel and blob approaches. B-splines are well known piecewise polynomial functions, and are characterized by the degree of their constituting polynomials. Recent works in sampling theory [18] [19] [15] have shown their efficiency in representing a continuous signal, with a good recovering accuracy. Increasing their degree makes them more and more similar to the 3D Gaussian functions, with a quasi-isotropic behaviour, while keeping local influence and separability property.

This gives us clues to develop a new efficient numerical projector for iterative reconstruction. One of the most important improvements we get is the reduction of the angular sampling of projections without any loss of quality.

Such an improvement is particularly of interest in the case of dynamic gated X-ray CT, which can be considered as a tomographic reconstruction problem with very few projection data, and for which we show some preliminary results.

This work was supported by the MiTiV project (Méthodes Inverses pour le Traitement en Imagerie du Vivant), funded by the French ANR (N° ANR-09-EMER-008).

Fabien Momey is with the Centre de Recherche Astrophysique de Lyon - Observatoire de Lyon, Lyon, France, and with the Laboratoire Hubert Curien, Université Jean Monnet, Saint-Étienne, France (telephone: +33 478 868 546, e-mail: author fabien.momey@univ-lyon1.fr).

Loïc Denis is with the Laboratoire Hubert Curien.

Catherine Mennessier is with the Laboratoire Hubert Curien, and with the engineer school CPE, Lyon, France.

Éric Thiébaut is with the Centre de Recherche Astrophysique de Lyon - Observatoire de Lyon.

Jean-Marie Becker is with the Laboratoire Hubert Curien, and with CPE Lyon.

Laurent Desbat is with the TIMC-IMAG, Grenoble, France.

II. Materials and Methods

A. Use of B-splines for image representation

Let $f : \boldsymbol{x} \mapsto f(\boldsymbol{x})$, with $\boldsymbol{x} = (x_1, x_2, \ldots, x_n) \in \mathbb{R}^n$, be the n-dimensional continuous function modelizing the true image to be reconstructed. Its decomposition on a discrete basis of functions gives:

$$f(\boldsymbol{x}) = \sum_{\boldsymbol{k}\in\mathbb{Z}^n} \mathrm{c}_{\boldsymbol{k}}\varphi_{\boldsymbol{k}}(\boldsymbol{x}) = \sum_{\boldsymbol{k}\in\mathbb{Z}^n} \mathrm{c}_{\boldsymbol{k}}\varphi(\boldsymbol{x}-\boldsymbol{x}_{\boldsymbol{k}}) \qquad (1)$$

where this discrete shift-invariant basis is assumed to be composed of the compact atom function $\varphi(\boldsymbol{x})$, regularly spaced on a n-dimensional grid of N samples. $\boldsymbol{k} = (k_1, k_2, \ldots, k_n)^{\mathrm{T}} \in \mathbb{Z}^n$ corresponds to indexes of the N samples of the discrete grid in the n-dimensional space, $\boldsymbol{x}_{\boldsymbol{k}} = (x_{k_1}, x_{k_2}, \ldots, x_{k_n})^{\mathrm{T}} \in \mathbb{R}^n$ are the coordinates of this discrete grid.

For numerical purposes, f is described as a vector of its N coefficients:

$$\mathbf{c} = (\mathrm{c}_{\mathbf{1}}, \mathrm{c}_{\mathbf{2}}, \ldots, \mathrm{c}_{\boldsymbol{N}})^{\mathrm{T}} \in \mathbb{R}^n \qquad (2)$$

The choice of the atom function φ of the basis is essential for warranting consistency with the image intrinsic continuity. It will be a key point for the design of the projector which has to modelize accurately the data.

B-splines are piecewise polynomial functions with degree d, continuously differentiable up to order $d-1$ [18]. Let $\beta^0(x)$ be the rectangular pulse. Thus β^d is a B-spline of degree d, constructed by d convolutions of β^0.

$$\beta^d(x) = \underbrace{\beta^0 * \cdots * \beta^0}_{d+1 \text{ terms}}(x) \qquad (3)$$

Hence going back to the formulation of the image representation in (1), we choose B-splines as our basis of functions φ, leading to:

$$f(\boldsymbol{x}) = \sum_{\boldsymbol{k}\in\mathbb{Z}^n} \mathrm{c}_{\boldsymbol{k}} \boldsymbol{\beta}^d_{\boldsymbol{k}}(\boldsymbol{x}) = \sum_{\boldsymbol{k}\in\mathbb{Z}^n} \mathrm{c}_{\boldsymbol{k}} \boldsymbol{\beta}^d(\boldsymbol{x} - \boldsymbol{x}_{\boldsymbol{k}}) \tag{4}$$

Classical basis functions used by some existing projectors are the simple staircase voxels. This is the case for the *distance driven* projector [1]. These functions are advantageous for being the most compact B-splines (of degree 0), easy to manipulate. However, staircase voxels suffer from a high anisotropic behaviour. They constitute a too coarse basis of representation of a continuous object, leading to large modelization errors. A finer sampling rate lowers these errors, but at the cost of an increased computational burden.

The accuracy of the model can be improved using B-splines of higher degree. Indeed B-splines are close to a Gaussian function when their degree d is large. Thus they tend to spherically symmetric function, while preserving a local support. As a result we can deal with quasi-isotropic functions. We also get a better approximation order in the modelization of $f(\boldsymbol{x})$. These two properties are related by the fact that B-splines are the shortest and smoothest scaling functions for a given order of approximation [19].

B. Projector

We consider a general tridimensional system with coordinates $\boldsymbol{x} = (x, y, z)$ linked to the object of interest. The regular sampling grid is therefore identified by the samples positions $\boldsymbol{x}_{\boldsymbol{k}}$, corresponding also to the center of each basis function $\boldsymbol{\beta}^d_{\boldsymbol{k}}$. Then we consider a flat detector, with coordinates $\boldsymbol{u} = (u, v)$. The detector acquires the projection with a given orientation denoted θ. Let $\mathbf{c}$ be the vector of coefficients of the image, defined in (2). The numerical data modelization at orientation θ is:

$$\mathbf{g}^\theta = \mathbf{R}^\theta \cdot \mathbf{c}\ , \quad \mathrm{g}^\theta_q = \sum_{k\in\Omega^\theta_q} \mathbf{R}^\theta_{qk} \cdot \mathrm{c}_k \tag{5}$$

where $\mathbf{R}^\theta$ is the projector and $\mathbf{g}^\theta$ is the resulting data vector, the elements of which are noted g^θ_q. The coefficient $\mathbf{R}^\theta_{qk}$ of the matrix $\mathbf{R}^\theta$ is the contribution of the voxel function k on the q^{th} data element. Ω^θ_q is the set of voxels k impinging the θ-oriented detector pixel q. Let $P_q : \boldsymbol{u} \mapsto P_q(\boldsymbol{u}) = \boldsymbol{\beta}^0(\boldsymbol{u} - \boldsymbol{u}_q)$ be the q^{th} detector pixel response, assumed to be a 2D rectangular pulse, centered at position $\boldsymbol{u}_q$. This response is shift-invariant over each detector pixel. Thus:

$$\mathbf{R}^\theta_{qk} = \int\!\!\int\ F^\theta_{\boldsymbol{k}}(\boldsymbol{u}) \cdot P_q(\boldsymbol{u})\ d\boldsymbol{u} \tag{6}$$

$F^\theta_{\boldsymbol{k}}$ is the footprint of the basis function $\boldsymbol{\beta}^d_{\boldsymbol{k}}$. It is nothing else than the X-ray transform of this function on the θ-oriented detector, along each ray trajectory $\{S(\theta), \vec{r}(\theta, \boldsymbol{u})\}$ crossing it, and impinging the detector plane at the position $\boldsymbol{u}$.

$$F^\theta_{\boldsymbol{k}}(\boldsymbol{u}) = \int_{\boldsymbol{x}\in\{S(\theta),\vec{r}(\theta,\boldsymbol{u})\}} \boldsymbol{\beta}^d_{\boldsymbol{k}}(\boldsymbol{x})\ d\boldsymbol{x} \tag{7}$$

A given projector $\mathbf{R}^\theta$ determines the expression of this footprint $F^\theta_{\boldsymbol{k}}$. Obviously, $F^\theta_{\boldsymbol{k}}$ depends on the chosen basis of functions. Moreover some approximations are often made in the calculation of this footprint and its contribution to detector pixels, in order to lower the computation cost.

Our approach uses the quasi-isotropy property of B-splines of higher degree, stated in section II-A, to suppose that the footprint is identical whatever the orientation θ. As a result, we first state that the footprint of $\boldsymbol{\beta}^d_{\boldsymbol{k}}$, in parallel beam geometry, is a $n-1$-dimensional B-spline of degree d, separable over the detector axis. For the 3D case, this gives:

$$F^\theta_{\boldsymbol{k}}(\boldsymbol{u}) = \beta^d(u - u_k) \cdot \beta^d(v - v_k) \tag{8}$$

where $(u_k, v_k) = \boldsymbol{u}_{\boldsymbol{k}}$ is the position, on the detector, of the projection of the center $\boldsymbol{x}_{\boldsymbol{k}}$ of $\boldsymbol{\beta}^d_{\boldsymbol{k}}$.

In the case of cone beam geometry, the magnification effect has to be taken into account, as well as the distorsion effect depending on the position of the voxel in the field of view. For the 3D case, this gives:

$$F^\theta_{\boldsymbol{k}}(\boldsymbol{u}) = \beta^d\left(\frac{u}{\Gamma^\theta_S \cdot \delta_{u_{\boldsymbol{k}}}} - u_{\boldsymbol{k}}\right) \cdot \beta^d\left(\frac{v}{\Gamma^\theta_S \cdot \delta_{v_{\boldsymbol{k}}}} - v_{\boldsymbol{k}}\right) \tag{9}$$

Γ^θ_S is the magnification factor; δ_{u_k} et δ_{v_k} are the distorsion factors.

A study of modelization and approximation errors of our model, compared with the *distance driven* model, has been done previously in [12], and has proven its better accuracy. We have shown that the use of cubic B-splines (degree 3) already reaches almost the best accuracy. However such a gain is at the cost of an increase of the required number of operations, due to the larger footprint of a given voxel as a function of the B-spline degree, as shown in Fig.1. But at the degree 3, it is only about 6 times larger, which remains is the same range of computational burden. Moreover our projection scheme, as well as the staircase voxel based approaches, is highly parallelizable, making possible to optimize the implementation for speeding up the calculation.

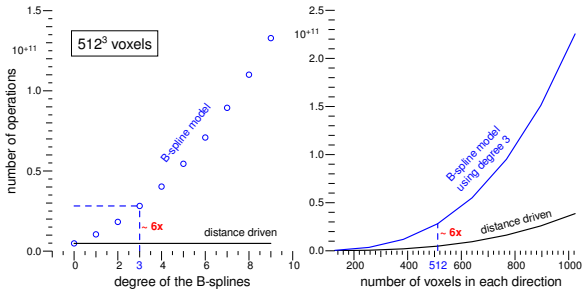

Fig. 1. Number of operations involved in the calculation of the 3D B-spline based projector, as a function of the B-spline degree and the number of voxels in each direction, compared with the *distance driven* projector.

III. Results on 2D fan beam reconstructions

A linear detector, linked to the fan beam source, is considered. The set source-detector rotates around the 2-dimensional object of interest. The B-spline coefficients of the image $\mathbf{c}$,

are reconstructed from the set of projections $\mathbf{g} = \{\mathbf{g}^\theta | \theta \in \Theta\}$, where Θ is the set of projection angles, by minimization of:

$$\mathbf{c} = \underset{\hat{\mathbf{c}}}{argmin} \underbrace{\sum_{\theta \in \Theta} ||\mathbf{g}^\theta - \mathbf{R}^\theta \cdot \hat{\mathbf{c}}||^2_{\mathbf{W}}}_{\text{data residuals}} + \underbrace{\mu \cdot \Psi(\mathbf{\Phi} \cdot \hat{\mathbf{c}})}_{\text{regularization term}} \quad (10)$$

where $||\cdot||^2_{\mathbf{W}}$ corresponds to the weighted least squares term. The weighting matrix $\mathbf{W}$ is the inverse of the noise covariance. $\Psi : \mathbf{f} \mapsto \Psi(\mathbf{f})$ is a regularization operator applied to the image in the samples space. The interpolation operator $\mathbf{\Phi}$, which transforms the B-spline coefficients in samples values, can be applied using fast digital filtering operations [16] [17] [18], as well as its inverse. Thus the additional computational burden is negligible. The regularization we use is a relaxed total variation prior [14]. The minimization of (10) is performed with a quasi-Newton optimization algorithm: the L-BFGS method [13].

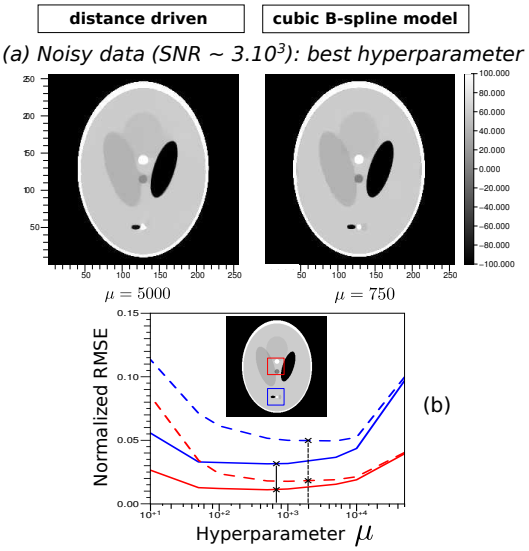

Fig. 2. (a) Reconstructions of a Shepp-Logan phantom 256×256, from a set of 60 projections with 512 detector pixels, with both the B-spline projector using cubic B-splines and the *distance driven* projector. Visualization in Hounsfield units. Reconstructions from noisy data (additional non-stationary Gaussian noise with a signal to noise ratio of about 3000), obtained with the value of μ giving the best visual image quality. (b) Normalized root mean square error in 2 regions of interest (ROI) of the reconstructed image, for various values of the hyperparameter μ (logarithmic scale). The ROIs are indicated on the image, with the corresponding color on the graphs. Solid curves : reconstructions with the B-spline projector. Dashed curves : reconstructions with the *distance driven* projector.

Fig.2 shows some of the previous results obtained in [12]. We had reconstructed a 256×256 Shepp-Logan phantom, from a set of 60 projections with 512 detector pixels, calculated analytically. The sampling rate was the same for both voxels and detector pixels. The reconstructions were performed with both our B-spline based projector, using cubic B-splines, and the *distance driven* projector, for comparison. The data were corrupted by a non-stationary Gaussian noise, with a signal to noise ratio approximately 3000.

Fig.2(a) displays some reconstructed images, obtained in [12]. The best value of the hyperparameter μ is found, which gives the best qualitative visual quality of the reconstructed image. Our B-spline based projector leads to a better image quality than *distance driven*, without regularizing a lot. Fig.2(b) shows curves of the normalized root mean square error (RMSE), calculated on 2 regions of interest (ROI) taken on the image, as a function of the hyperparameter μ, using both the B-spline based projector using cubic B-splines (solid curves) and the *distance driven* projector (dashed curves). The curves show that, for each ROI, the B-spline based projector's RMSE is always lower than the *distance driven* projector's RMSE. Thus for this given evaluation metric, our projector shows again the best performances.

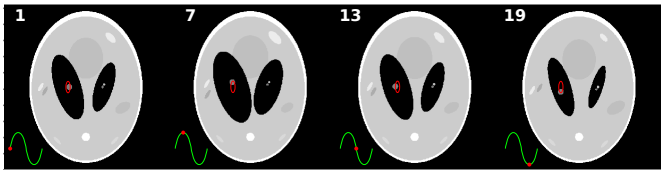

Fig. 3. Dynamic Shepp-Logan phantom 512×512. A 5 seconds period of motion is chosen and 25 frames are extracted. The frames 1, 7, 13 and 19 are represented. The position of each frame's date in the temporal sinusoidal signal is indicated. The red ellipse corresponds to the trajectory of the small circular insert in the left big ellipse distorted over time.

IV. Application on simulated 2D dynamic X-ray gated CT

We experiment our projector in the context of dynamic X-ray tomography. More precisely we simulate a 2D case of gated iterative reconstruction of a Shepp-Logan phantom, some ellipses of which see its parameters periodically moving over time (semi-minor or major axis, center's position). Hence the motion of the phantom's ellipses can be either translations or distorsions. The temporal signal associated to the periodic variation of the parameters is a sinus function, that is to say that the speed of motion is not constant over a period. Fig.3 shows frames of the simulated object. Each frame's size is 512×512. The speed of the motion is almost the fastest for frames 1 and 13, and almost the slowest for frames 7 and 19. For instance the trajectory of motion of the small circular insert in the left big ellipse is indicated on Fig.3 for illustration. The position of the frame's date in the temporal sinusoidal signal is also indicated.

The geometry of the acquisition system is the same as in III, but now a period is defined for a whole rotation of the detector around the object. We choose this acquisition time to be equal to 120 seconds. During this period, 600 projections, regularly spaced in time, and on 360°, are simulated analytically from the state of the object at the corresponding date. The period of motion lasts 5 seconds. As a result 24 periods of motion occur during the acquisition. We want to be in gated mode, so we reconstruct 25 frames of a period of motion of the object, such that a given projection is exactly registered to a given frame. Hence we have 25 frames, each one repeated 24 times during the acquisition, thus associated with 24 projections regularly spaced on 360°. It is very important to notice that this problem results in reconstructing each frame from very angularly undersampled data.

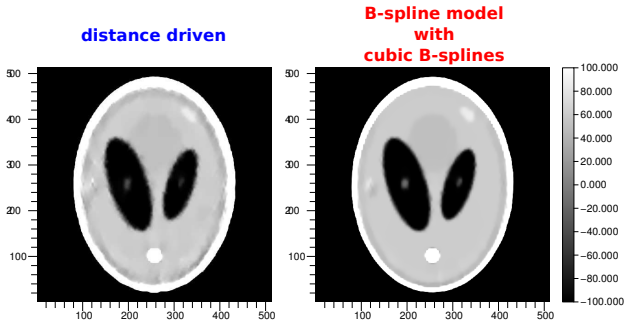

Fig. 4. Frame 13 of the reconstructed gated 128×128 Shepp-Logan sequence, with both the B-spline projector using cubic B-splines (right) and the *distance driven* projector (left). The reconstructed images are re-interpolated on a finer 512×512 grid, using cubic B-spline interpolator.

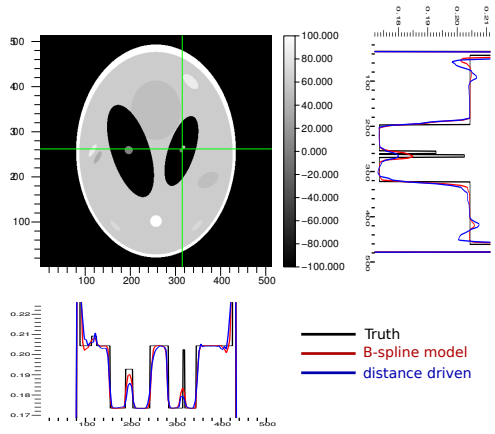

Fig. 5. Horizontal and vertical profiles taken on frame 13 of the reconstructed gated 128×128 Shepp-Logan sequence, with both the B-spline projector using cubic B-splines (right) and the *distance driven* projector (left). The reconstructed images are re-interpolated on a finer 512×512 grid, using cubic B-spline interpolator.

From this set of projections, we perform gated reconstructions of the 25 frames. The reconstruction of this sequence is performed globally, each frame reconstruction following the same optimization scheme as in Eq.10, for the data residuals' part. A global spatio-temporal regularization is performed on the "2D + time" sequence, which consists in the same regularizer used in III, but extended to 3 dimensions to take into account the temporal correlation between frames.

Fig.4 shows preliminary results of reconstructions, with both our B-spline based projector, using cubic B-splines, and the *distance driven* projector, for comparison. We focus our visualization on a single frame, the 13^{th}, at which the speed of the motion is faster. The reconstructed 128×128 images are re-interpolated on a finer 512×512 grid, using a cubic B-spline interpolator, for a better image quality. We can see the better visual quality of the frame reconstructed with our B-spline projector.

Fig.5 shows profiles of the reconstructions shown in Fig.4, for a more precise evaluation. Again the superior ability of our projector to recover finer details is visible.

V. Conclusion and further works

We have presented a new type of numerical projector for iterative reconstruction in tomography. It is based on the use of a basis of separable 3D B-splines, which is much more adapted for data modelization than the staircase voxels.

We have demonstrated the better accuracy of our projector based on cubic B-splines, on 2-dimensional regularized iterative reconstructions, from simulated data, using a small number of projections, compared with the *distance driven* projector.

We also have studied its behaviour in the context of dynamic gated X-ray tomography. The fact that the temporal dimension has to be included in the reconstructed image, i.e. it becomes a "2D + time" image, reduces drastically the number of projections available for a given temporal frame. Preliminary results have again shown that the accuracy of the projector is a key point to deal with this lack of data in the reconstruction process, and to make the best use of available information.

References

[1] B. DeMan and S. Basu. *Distance driven projection and backprojection in three dimensions*. Physics in Medicine and Biology, 2004, 49, p2463-2475.

[2] J.A. Fessler. *Iterative methods for image reconstruction*. IEEE International Symposium on Biomedical Imaging Tutorial, Arlington Virginia, 2006.

[3] Y. Long, J.A. Fessler and J.M. Balter. *3D Forward and Back-Projection for X-Ray CT Using Separable Footprints*. IEEE Transactions on Medical Imaging, 2010, 29, p1839-1850.

[4] S. Horbelt, M. Liebling and M. Unser. *Discretization of the Radon transform and of its inverse by spline convolutions*. IEEE Transactions on medical imaging, 2002, 21, p363-376.

[5] P.M. Joseph. *An improved algorithm for reprojecting rays through pixel images*. IEEE Transactions on Medical Imaging, 1982, 1, p192-196.

[6] M. Slaney and A. Kak. *Principles of computerized tomographic imaging*. SIAM, Philadelphia, 1988.

[7] R.M. Lewitt. *Multidimensional digital image representations using generalized Kaiser-Bessel window functions*. JOSA A, 1990, 7, p1834-1846.

[8] R.M. Lewitt. *Alternatives to voxels for image representation in iterative reconstruction algorithms*. Physics in Medicine and Biology, 1992, 37, p705-716.

[9] S. Matej and R.M. Lewitt. *Image representation and tomographic reconstruction using spherically symmetric volume elements*. IEEE Medical Imaging Conference Record, 1992, p1191-1193.

[10] S. Matej and R.M. Lewitt. *Efficient 3D grids for image reconstruction using spherically-symmetric volume elements*. IEEE Transactions on Medical Imaging, 1995, 42, p1361-1370.

[11] S. Matej and R.M. Lewitt. *Practical considerations for 3D image reconstruction using spherically symmetric volume elements*. IEEE Transactions on Medical Imaging, 1996, 15, p68-78.

[12] F. Momey, L. Denis, C. Mennessier, É. Thiébaut, J.M. Becker and L. Desbat. *A new representation and projection model for tomography, based on separable B-splines*. IEEE Medical Imaging Conference Record, 2011, p2602-2609.

[13] J. Nocedal. *Updating quasi-Newton matrices with limited storage*. Mathematics of computation, 1980, 35, p773-782.

[14] L.I. Rudin, S. Osher and E. Fatemi. *Nonlinear total variation based noise removal algorithms*. Physica D: Nonlinear Phenomena, 1992, 60, p259-268.

[15] P. Thévenaz, T. Blu and M. Unser. *Interpolation Revisited*. IEEE Transactions on Medical Imaging, 2000, 19, p739-758.

[16] M. Unser., A. Aldroubi and M. Eden. *B-spline signal processing: Part I-Theory*. IEEE Transactions on Signal Processing, 1993, 41, p821-833.

[17] M. Unser., A. Aldroubi and M. Eden. *B-spline signal processing: Part II-Efficient design and applications*. IEEE Transactions on Signal Processing, 1993, 41, p834-848.

[18] M. Unser. *Splines: A perfect fit for signal and image processing*. IEEE Signal Processing Mag., 1999, 16, p22-38.

[19] M. Unser. *Sampling-50 years after Shannon*. Proceedings of the IEEE, 2000, 88, p569-587.